Journal of Marine Research, 65, 317–343, 2007

Journal of MARINE RESEARCH

Volume 65, Number 3

A fast numerical solution to the general mass-conservation equation for solutes and solids in aquatic sediments

by Peter Berg[1], Dennis Swaney[2], Søren Rysgaard[3], Bo Thamdrup[4] and Henrik Fossing[5]

ABSTRACT

Mathematical modeling of species transformations in aquatic sediments is usually based on numerical solutions to the same general one-dimensional mass-conservation equation and is likely to require substantial computation time. In this paper we present a fast numerical solution to this equation. The solution is suited for both single and multi-component models and it is based on an implicit control volume discretization of the general mass-conservation equation. The solution consists of two algorithms, one that decomposes the discretization matrix once and one that subsequently produces multiple solutions with minimal computational effort. A unique feature of these algorithms is that values of boundary conditions can vary as a simulation progresses without requiring new decompositions of the discretization matrix. This feature can reduce computation time significantly relative to commonly used procedures for modeling dynamic systems. Finally, we present four examples in which the numerical solution is applied to specific problems. From these examples guidelines are derived for the discretization in space and time required to obtain precise solutions of the general mass-conservation equation.

1. Introduction

The numerical mathematical models that are being used extensively to study biogeochemical transformations in aquatic sediments typically rely on a one-dimensional mass-

1. Department of Environmental Sciences, University of Virginia, Charlottesville, Virginia, 22903, U.S.A. ***email: pb8n@virginia.edu***

2. Department of Ecology and Evolutional Biology, Cornell University, Ithaca, New York, 14853, U.S.A.

3. Greenland Institute of Natural Resources, Kiviog 2, Box 570, 3900 Nuuk, Greenland.

4. Danish Center for Earth System Science, Institute of Biology, University of Southern Denmark, Campusvej 55, DK-5230 Odense M., Denmark.

5. National Environmental Research Institute, Aarhus University, Department of Marine Ecology, Vejlsøvej 25, DK 8600 Silkeborg, Denmark.

conservation approach and include the vertical transport of one or more species. For example, many multi-component models have been published on organic matter and nutrient diagenesis (i.e., Rysgaard and Berg, 1996; Boudreau, 1996; Dhakar and Burdige, 1996; Soetaert *et al*., 1996; Van Cappellen and Wang, 1996; Luff *et al*., 2000; Berg *et al*., 2003; Meysman *et al*., 2003). Single-component models also generally require a numerical approach, for example as a tool to interpret measured concentration-depth profiles of ^{210}Pb when estimating rates of sedimentation and bioturbation (i.e., Mulsow *et al*., 1998; Berg *et al*., 2001), or for extractions of production and consumption rates from measured concentration-depth profiles (i.e., Berg *et al*., 1998; Meile *et al*., 2001). A key element in all these studies is a numerical solution to the same general one-dimensional mass-conservation equation. The equation that includes transient and steady-state conditions, dissolved and solid species, solutes that adsorb onto the solid sediment, and the transport contributions by molecular diffusion, bioturbation (described as a diffusive process), irrigation (described as a non-local transport), and advection, yields

$$(\xi\varphi + \rho_s(1-\varphi)\kappa)\frac{\partial C}{\partial t} = \frac{\partial}{\partial x}\left((\xi\varphi(D_{Bw} + D_s) + \rho_s(1-\varphi)D_{Bs}\kappa)\frac{\partial C}{\partial x}\right) - \frac{\partial}{\partial x}((\xi(\varphi u)_x + \rho_s((1-\varphi)w)_x\kappa)C) + \xi\varphi\alpha(C_0 - C) + (R_1 + R_2 C) \quad (1)$$

where φ is the porosity, ρ_s is the density of the solid sediment, C is the concentration, t is the time, x is the depth, D_{Bw} is the biodiffusivity for solutes, D_s is the molecular diffusivity corrected for tortuosity, D_{Bs} is the biodiffusivity for solids, u is the pore water velocity relative to the sediment-water interface, w is the velocity of solids relative to the sediment-water interface, α is the irrigation coefficient, C_0 is the water column concentration, R_1 is the net production rate per unit volume of sediment, and R_2 is the rate constant for the first order production term. The parameters ξ and κ indicate whether the species is a solute ($\xi = 1$, $\kappa = 0$), a solid ($\xi = 0$, $\kappa = 1$), or a solute that adsorb to the solid sediment ($\xi = 1$, $\kappa = K'$ where K' is the adsorption constant). Different biodiffusivities are defined for solutes and solids in Eq. 1 based on recent studies of Berg *et al*. (2001, 2003) indicating that the effects of bioturbation on solutes can be many fold stronger than on solids. Adsorption (and desorption) of solutes onto the solid sediment is included as a reversible process assumed to be in local equilibrium at any time in a depth-to-depth comparison. As a result of continuity conditions for the pore water and the solid fraction of the sediment ($\partial(\varphi u)/\partial x = 0$, $\partial((1-\varphi)w)/\partial x = 0$), the products φu and $(1-\varphi)w$ are constant with depth. As a result, each of the terms φu and $(1-\varphi)w$ can be evaluated at any depth as indicated with the notation $(\,)_x$ in Eq. 1. For further details on Eq. 1, see for example Berner (1980) and Boudreau (1997).

Modeling of organic matter and nutrient diagenesis often requires significant computation times. For example, Van Cappellen and Wang (1996) ran their model on a SUN Sparc Station IPX which required 30 min to produce one single steady-state solution. Along the same lines, Luff *et al*. (2000) vectorized their code so it was suited to run on a CRAY

vector processor in order to reduce computation time. The fact that such models usually are run numerous times when applied to specific sediments or when used in analysis underscores the importance of choosing the numerical solution algorithm carefully. Models used as interpretation tools can also require substantial computational effort. For example, the procedure PROFILE (Berg *et al*., 1998) often simulates 10^6-10^7 independent steady-state profiles in the interpretation of a single measured concentration-depth profile.

This paper presents a numerical solution to Eq. 1 that is developed specifically to minimize computation time. The algorithm is suited to both single and multi-component models, and when utilized it can reduce computation time significantly relative to that of commonly used procedures. For that reason, it allows models as outlined above to be implemented on standard microcomputers (desktop and laptop computers) without resulting in prohibitive computation times.

2. Numerical solution

The numerical solution to Eq. 1 is based on a control volume approach (Patankar, 1980) and relies on a separation of the calculation domain into N control volumes each containing a grid point at its center (Fig. 1). It is assumed that the variation in space and time of concentration, C, is described by piecewise continuous profiles which are uniquely determined when the grid point values of C are known. A discretization equation is derived using these profiles in an integration of Eq. 1 over a time step and a control volume. One clear advantage of this control volume approach is that mass-conservation is fulfilled exactly in the discretization equation.

a. Discretization equation

The user-defined control volumes comprising the calculation domain can vary with depth, allowing a fine resolution to be used near the sediment-water interface where the most pronounced gradients and second derivatives of concentrations are expected. The thickness of control volumes 1 and N are zero by definition (Fig. 1). If a diffusive boundary layer is included in the calculation domain, a control volume indexed M with a thickness of zero, marks the sediment-water interface. If this control volume separation is used for multi-component models involving both dissolved and solid species, solute concentrations are described for control volume 1 to N while concentrations of solids are found for control volume M to N.

The integration of Eq. 1 over a time step, from time t to $t + \Delta t$, and over control volume j, from $x_{j-1/2}$ to $x_{j+1/2}$, yields

$$\int_{x_{j-1/2}}^{x_{j+1/2}} \int_{t}^{t+\Delta t} H_1 \frac{\partial C}{\partial t}\, dt\, dx = \int_{x_{j-1/2}}^{x_{j+1/2}} \int_{t}^{t+\Delta t} \left(\frac{\partial}{\partial x} \left(H_2 \frac{\partial C}{\partial x} - H_3 C \right) + H_4(C_0 - C) + (R_1 + R_2 C) \right) dt\, dx \tag{2}$$

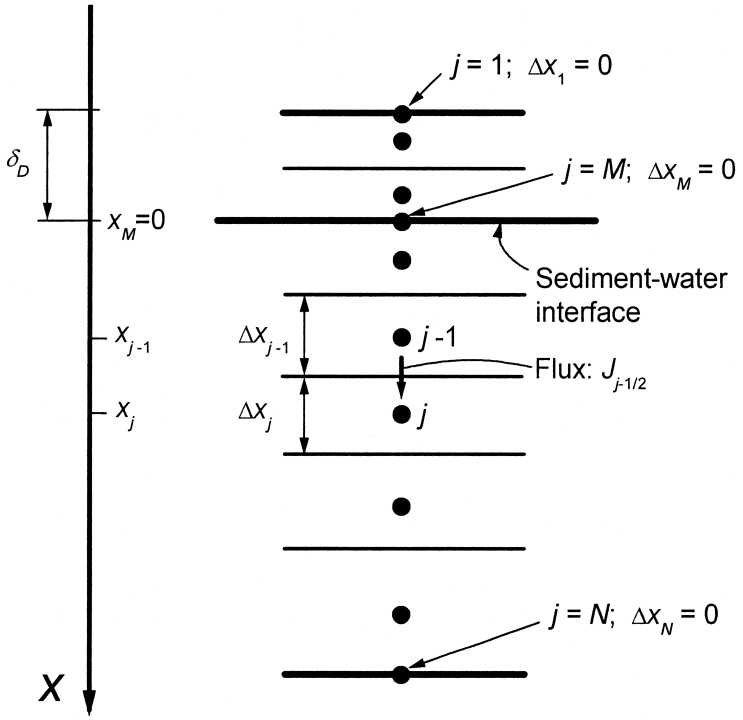

Figure 1. Separation of the water-sediment column into control volumes for a situation when the diffusive boundary layer, δ_D, is included in the calculations. Note that size of control volume 1, *M*, and *N* are zero.

where

$$
\begin{aligned}
H_1 &= \xi\varphi + \rho_s(1-\varphi)\kappa \\
H_2 &= \xi\varphi(D_{Bw} + D_s) + \rho_s(1-\varphi)D_{Bs}\kappa \\
H_3 &= \xi(\varphi u)_x + \rho_s((1-\varphi)w)_x\kappa \\
H_4 &= \xi\varphi\alpha
\end{aligned}
\tag{3}
$$

The variables H_1, H_2, and H_4 can vary with depth while H_3 as a result of continuity always will be constant with depth.

In order to perform the integration in Eq. 2, it is now assumed that H_1, H_2, H_3, H_4, R_1, and R_2 are constant throughout the time step and that the grid point values of H_1, H_4, R_1, and R_2 prevail throughout the control volume as representative mean values. The latter assumption is not needed for H_2 and H_3 because these variables are not integrated over the control volume. With these assumptions Eq. 2 gives

$$H_{1j}(C_j^{n+1} - C_j^n)\Delta x_j = \int_t^{t+\Delta t} \left(\left(H_2 \frac{\partial C}{\partial x} - H_3 C \right)_{j+1/2} - \left(H_2 \frac{\partial C}{\partial x} - H_3 C \right)_{j-1/2} + (H_{4j}(C_0 - C_j) + (R_{1j} + R_{2j} C_j))\Delta x_j \right) dt \quad (4)$$

where C_j^n is the old (known) grid point value of C at time t, and C_j^{n+1} is the new (unknown) grid point value of C at time $t + \Delta t$.

The second term on the right side of Eq. 4, $-(H_2 \partial C/\partial x - H_3 C)_{j-1/2}$, represents the combined diffusive-advective flux, $J_{j-1/2}$, over the boundary between control volume j-1 and j (Fig. 1). It has long been known that a straightforward central difference approximation of $J_{j-1/2}$ inevitably leads to numerical instability when modeling advection-dominated systems (Courant *et al.,* 1952). For that reason researchers have suggested approximations of $J_{j-1/2}$ that ensure unconditionally stable schemes (i.e., Courant *et al.*, 1952; Spalding, 1972; Fiadeiro and Veronis, 1977; Patankar, 1980, 1981; Berg, 1985). Some of the most successful schemes were derived as approximations to the analytical solution to the one-dimensional steady state mass-conservation equation accounting for transport by diffusion and advection. These schemes were defined through the 1970s and early 1980s and their success was evaluated not only in terms of how well they approximated this analytical solution but also how fast they could be evaluated numerically. Because computer processors have changed radically since then the relative utility of these evaluation schemes have changed as well. For this reason, we compare the performance of a selection of the most popular schemes on a modern microcomputer in Appendix A.

Common to all these schemes is the expression of flux, $J_{j-1/2}$, as

$$J_{j-1/2} = F_{1j} C_j + F_{2j} C_{j-1} \quad (5)$$

and the individual schemes are defined through their definition of F_{1j} and F_{2j} which are derived in details for these schemes in Appendix A. Combining Eqs. 4 and 5 gives

$$H_{1j}(C_j^{n+1} - C_j^n)\Delta x_j = \int_t^{t+\Delta t} (-F_{1j+1} C_{j+1} - F_{2j+1} C_j + F_{1j} C_j + F_{2j} C_{j-1} + (H_{4j}(C_0 - C_j) + (R_{1j} + R_{2j} C_j))\Delta x_j) dt \quad (6)$$

When approximating the time integral in Eq. 6, it is necessary to assume how all the time-dependent terms vary from time t to $t + \Delta t$. The time integral of C_j can be expressed as $((1 - \beta) C_j^n + \beta C_j^{n+1})\Delta t$ where β is a weighting factor, and different schemes will result depending on the value of β. With $\beta = 0$, an explicit scheme is obtained, while $\beta = 1$ leads to an implicit scheme. With $\beta = ½$, the Crank-Nicolson scheme, a well-known hybrid of the explicit and the implicit scheme, is obtained. The implicit scheme is chosen here for the following reasons. Firstly, it leads to a versatile numerical solution allowing

transient solutions to be found using appropriately sized time steps, and at the same time, allowing steady-state solutions to linear problems to be produced with minimal computational effort in one large time step. Secondly, the implicit scheme is especially attractive in one-dimensional formulations when computation time is of concern. While the number of numeric operations per time step in the explicit, Crank-Nicolson, and implicit scheme is similar, a restrictive upper limit exists for the time steps in the explicit scheme. When violated, numerical instability occurs. For example, in diffusion-dominated systems this critical time step equals $\frac{1}{2}\Delta x^2 H_1/H_2$ where H_1 and H_2 are given by Eq. 3. In models of organic matter and nutrient diagenesis where oxygen usually is a key component that typically penetrates only a few mm into the sediments, a Δx of $\sim$ 0.01 cm is required to accurately describe the oxygen profile. With typical values of H_1 and H_2 of 0.8 and 10^{-5} cm^2 s^{-1}, the critical time step is 4 s for the explicit scheme. Such small time steps will lead to prohibitive computation times when multiple-year simulations are required. Upper limits to the time step obviously also exist for the implicit scheme in such simulations, but they are of a different nature and are generally markedly less restrictive. For example, in multi-component models, fast non-linear reactions between species can restrict the size of the time steps that can be used. However, in such modeling exercises, performed with realistic reaction rate constants, time steps on the order of 1 h are usually sufficient to ensure an accurate numerical solution as we demonstrate in an example below. As the result of the explicit element in the Crank-Nicolson scheme it can, depending on the application, also suffer from restrictive demands on the time step. As a simple example of this, it is not possible to produce steady-state solutions to linear problems in one large time step as is the case with the implicit scheme.

The implicit time integration in Eq. 6 gives

$$H_{1j}(C_j^{n+1} - C_j^n)\frac{\Delta x_j}{\Delta t} = -F_{1\,j+1}C_{j+1}^{n+1} - F_{2\,j+1}C_j^{n+1} + F_{1\,j}C_j^{n+1} + F_{2\,j}C_{j-1}^{n+1} + H_{4j}(C_0 - C_j^{n+1})\Delta x_j + (R_{1\,j} + R_{2\,j}C_j^{n+1})\Delta x_j \tag{7}$$

which gives the following tri-diagonal system of equations

$$AA_jC_{j-1}^{n+1} + BB_jC_j^{n+1} + CC_jC_{j+1}^{n+1} = DD_j \tag{8}$$

where the coefficients are defined as

$$\begin{aligned} AA_j &= F_{2\,j} \\ BB_j &= F_{1\,j} - F_{2\,j+1} - H_{4j}\Delta x_j + R_{2\,j}\Delta x_j - H_{1\,j}\frac{\Delta x_j}{\Delta t} \\ CC_j &= -F_{1\,j+1} \\ DD_j &= -H_{1\,j}\frac{\Delta x_j}{\Delta t}C_j^n - H_{4j}C_0\Delta x_j - R_{1\,j}\Delta x_j \end{aligned} \tag{9}$$

Table 1. Definition of coefficients BB_L, CC_L, DD_L, AA_N, BB_N, and DD_N in Eq. 10 and 11 depending on the imposed type and value of boundary condition.

Upper boundary condition:	BB_L	CC_L	DD_L
Known concentration	1	0	The known concentration
Known flux	F_{2L+1}	F_{1L+1}	The known flux
Known gradient	$-2/\Delta x_{L+1}$	$2/\Delta x_{L+1}$	The known gradient
Lower boundary condition:	AA_N	BB_N	DD_N
Known concentration	0	1	The known concentration
Known flux	F_{2N}	F_{1N}	The known flux
Known gradient	$-2/\Delta x_{N-1}$	$2/\Delta x_{N-1}$	The known gradient

The control volume spanning Δx_j is included deliberately as a factor in Eq. 9 rather than a denominator allowing Δx_j to equal zero.

b. Boundary conditions

The boundary conditions that bring closure to the tri-diagonal system of equations (Eq. 7) are imposed implicitly through control volume L and N, where L equals either 1 or M depending on how the calculation domain is separated into control volumes (Fig. 1). For control volume L and N, Eq. 8 simplifies to

$$BB_L C_L^{n+1} + CC_L C_{L+1}^{n+1} = DD_L \tag{10}$$

and

$$AA_N C_{N-1}^{n+1} + BB_N C_N^{n+1} = DD_N. \tag{11}$$

The coefficients BB_L, CC_L, DD_L, AA_N, BB_N, and DD_N are given values depending on the kind of boundary conditions imposed. Three types of boundary conditions are possible: a known concentration, a known flux, and a known concentration gradient. The assignment of values to BB_L, CC_L, DD_L, AA_N, BB_N, and DD_N depending on the type and value of the boundary conditions are outlined in Table 1. The unique set of boundary concentrations, C_L^{n+1} and C_N^{n+1}, which ensures that the desired boundary conditions are imposed, is obtained when the tri-diagonal system of equations (Eqs. 8, 10, 11) is solved.

c. Solution of tri-diagonal system of equations

Several models of biogeochemical transformations in aquatic sediments rely on implicit schemes. In these models, the tri-diagonal system of equations is typically solved by Gaussian elimination numerous times in a single simulation (i.e. Dhakar and Burdige, 1996; Van Cappellen and Wang, 1996) using for example the Thomas algorithm (i.e. Patankar, 1980; Huyakorn and Pinder, 1983). Rather than performing this straightforward

Gaussian elimination in every time step, a significant reduction in computation time can be obtained as follows.

The coefficient DD_j in the tri-diagonal system of equations (Eq. 9, Table 1) will typically vary from time step to time step, in most applications simply because DD_j contains the concentration C_j^n at the old time level t. In contrast, the coefficients AA_j, BB_j and CC_j are likely to be constant throughout the simulation (Eq. 9, Table 1), or at least vary at such a slow rate that it is appropriate to treat them as constants through many consecutive time steps. An example of this is dynamic simulations based on time steps on the order of minutes and where much slower seasonal temperature variations will affect variables such as molecular diffusivities, and thus AA_j, BB_j and CC_j. In such simulations, it is clearly a good approximation only to update or recalculate the coefficients AA_j, BB_j and CC_j on a weekly or monthly basis. This characteristic can be taken advantage of to reduce the computational effort significantly in successive solutions of the tri-diagonal system of equations by decomposing the discretization matrix only once, or only with time intervals where AA_j, BB_j and CC_j vary markedly. This is done by reformulating the Thomas algorithm.

The forward substitution in the Thomas algorithm where Eqs. 8, 10, and 11 are solved in the interval $L \leq j \leq N$ yields (i.e. Patankar, 1980; Huyakorn and Pinder, 1983)

$$\begin{aligned} PP_L &= -\frac{CC_L}{BB_L}; \quad QQ_L = \frac{DD_L}{BB_L} \\ PP_j &= -\frac{CC_j}{BB_j + AA_j PP_{j-1}} \\ QQ_j &= \frac{DD_j - AA_j QQ_{j-1}}{BB_j + AA_j PP_{j-1}} \end{aligned} \Bigg\} \quad (j = L+1 \rightarrow N-1)$$

$$QQ_N = \frac{DD_N - AA_N QQ_{N-1}}{BB_N + AA_N PP_{N-1}} \tag{12}$$

where PP_j and QQ_j are decomposition variables and AA_j, BB_j, CC_j, and DD_j are defined either by Eq. 9 or in Table 1. The following back substitution that gives the values of C_j^{n+1} yields

$$\begin{aligned} C_N^{n+1} &= QQ_N \\ C_j^{n+1} &= PP_j C_{j+1}^{n+1} + QQ_j \quad (j = N-1 \rightarrow L) \end{aligned} \tag{13}$$

The significant gain in computational efficiency is now achieved by rewriting Eq. 12 so that DD_j is kept out of the forward substitution by defining an additional decomposition variable NN_j as follows:

$$NN_L = \frac{1}{BB_L}; \quad PP_L = -CC_L NN_L$$

$$\left.\begin{aligned} NN_j &= \frac{1}{BB_j + AA_j PP_{j-1}} \\ PP_j &= -CC_j NN_j \end{aligned}\right\} \quad (j = L+1 \rightarrow N-1) \tag{14}$$

$$NN_N = \frac{1}{BB_N + AA_N PP_{N-1}}$$

With this modification the back substitution that gives the values of C_j^{n+1} then yields

$$\begin{aligned} QQ_L &= DD_L NN_L \\ QQ_j &= (DD_j - AA_j QQ_{j-1}) NN_j \quad (j = L+1 \rightarrow N) \\ C_N^{n+1} &= QQ_N \\ C_j^{n+1} &= PP_j C_{j+1}^{n+1} + QQ_j \quad (j = N-1 \rightarrow L) \end{aligned} \tag{15}$$

There are $5(N - L) + 1$ numeric operations in Eq. 15, approximately half the number used in the original Thomas algorithm ($10(N - L) - 1$). Because multiplications are computationally less costly to perform than divisions, the overall result is that Eq. 15 are 2.5 times faster to execute than those of the original Thomas algorithm on a 2.0 GHz Pentium M PC.

Another important and unique feature of this numerical solution is that the type of boundary condition is introduced through BB_L, CC_L, AA_N, and BB_N (Table 1) while the values of the boundary condition are imposed through DD_L and DD_N. This characteristic allows the values of boundary conditions to vary as a simulation progresses without requiring new decompositions of the discretization matrix.

The coefficient DD_j (Eq. 9) must be calculated in every time step. This is done most effectively as

$$DD_j = -EE_j C_j^n - FF_j C_0 - R_{1\,j} \Delta x_j \tag{16}$$

where EE_j and FF_j are defined as

$$EE_j = H_{1\,j} \frac{\Delta x_j}{\Delta t} \quad \text{and} \quad FF_j = H_{4\,j} \Delta x_j \tag{17}$$

which, with the definitions of $H_{1\,j}$ and $H_{4\,j}$ (Eq. 3), typically need only be evaluated once.

In summary, it is convenient to calculate the coefficients given by Eqs. 3, 9, and 17 and perform the new forward substitution given by Eq. 14 in one algorithm. We have named this algorithm CONSTANTS and its content is summarized in Appendix B. The algorithm includes five optional expressions for the molecular sediment diffusivity (D_s) as a function of porosity and diffusivity in water. The two first were originally defined by Ullman and Aller (1982), the third and fourth were given by Iversen and Jørgensen (1993), and the fifth

was defined by Boudreau (1997). The output from CONSTANTS are input to the second algorithm, CNEW, which performs the back substitution (Eq. 15) leading to the new concentrations every time it is utilized. The content of CNEW is summarized in Appendix C.

3. Applications and examples

The numerical solution, separated into the two algorithms CONSTANTS and CNEW, is rather versatile and can be used to simulate steady state, dynamic, linear, and nonlinear problems that further can involve one or more dissolved or solid species. The outlined features of the solution are particularly beneficial in applications where long computation times are of concern.

Four example applications of the algorithm are presented below, representing computational gains achieved in diverse problems. The first three focus on rather simple cases, for which analytical solutions exist. They also serve as a test of the numerical solution and as an illustration of the discretization in depth, (and in time for transient problems) required to obtain accurate solutions. In the last example, the solution is implemented in a dynamic, multi-component, and nonlinear model of organic matter and nutrient diagenesis in a specific sediment. This example illustrates clearly the significant advantages that can be achieved in terms of short computation times when applying the numerical solution to models where components with very different time constants require relatively small time steps combined with long simulation times to produce quasi-stationary solution on a year to year basis. All examples are coded in FORTRAN 90 and the simulations are performed in double precision.

a. Example 1

Four types of solute transport, molecular diffusion, bioturbation, irrigation, and advection, are represented in Eq. 1. An analytical solution to the equation is possible under steady-state conditions if advection and first-order production terms are neglected, and if φ, D_s, D_{Bw}, α, and R_1 are assumed to be constant with depth. Under these conditions Eq. 1 simplifies to

$$\varphi(D_{Bw} + D_s)\frac{d^2C}{dx^2} + \varphi\alpha(C_0 - C) + R_1 = 0 \tag{18}$$

which has the solution

$$C = A\,\exp\left(-\sqrt{\frac{\alpha}{D_{Bw} + D_s}}\,x\right) + B\exp\left(\sqrt{\frac{\alpha}{D_{Bw} + D_s}}\,x\right) + \frac{\alpha C_0 + \dfrac{R_1}{\varphi}}{\alpha} \tag{19}$$

where A and B are arbitrary constants (Boudreau 1997).

Berg *et al*. (1998) calculated a hypothetical O_2 profile in the depth interval from -0.05 to 1.0 cm assuming constant consumption rates (R_1) of 0.004 and 0.012 nmol cm^{-3} s^{-1} for the depth intervals of 0 to 0.75 and 0.75 to 1.0 cm and then applying Eq. 19 to each of these

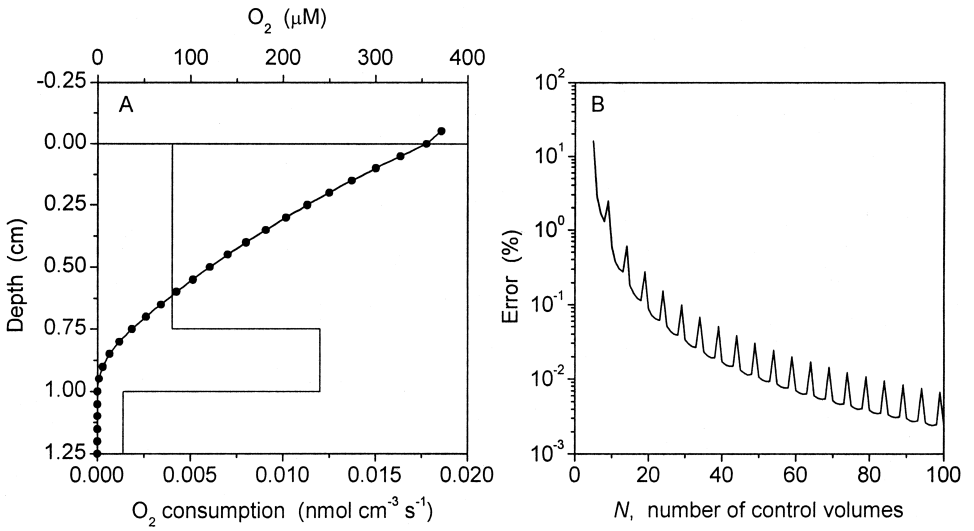

Figure 2. (A) Hypothetical steady state O_2 depth-profile defined analytically (dots) and simulated numerically by utilizing the algorithms CONSTANTS and CNEW (line). The imposed O_2 consumption varies with depth (step function). (B) The error of the numerical solution for different numbers of equally spaced control volumes separating the -0.05 to 1.25 cm depth interval.

intervals. In the diffusive boundary layer (δ_D) from -0.05 to 0 cm, the solution simplifies to a straight line. It was further assumed that the O_2 concentration equals 0 at 1 cm depths and below. Finally, values of φ, D_{Bw}, D_s, and α, of 0.75, 3×10^{-6} cm^2 s^{-1}, 9×10^{-6} cm^2 s^{-1}, and 5×10^{-6} s^{-1} were assumed by Berg *et al.* (1998). Here (Fig. 2A) we extended the solution to also include the depth interval of 1 to 1.25 cm for which Eq. 18 simplifies to $R_1 = -\varphi\alpha C_0$.

The O_2 profile was simulated repeatedly utilizing the algorithms CONSTANTS and CNEW while the number of equally spaced control volumes (N) was increased incrementally. The error of the numerical solution was determined as the maximum deviation in the -0.05 to 1.25 cm depth interval from the analytical solution in percent of the water column concentration (Fig. 2B). Since the numerical solution is fully implicit each simulated steady-state profile was determined in one single use of both CONSTANTS and CNEW in which an "infinitely large" time step (1×10^{30} s) was specified. The error of the numerical solution declines rapidly with increasing N (Fig. 2B) and errors < 1, 0.1, and 0.01% was found for N equal to 10, 25, and 80. The local periodic variation of the error was caused by offsets between the abrupt changes in the imposed O_2 consumptions (Fig. 2A) and the boundaries between control volumes.

b. Example 2

Two types of solid transport, bioturbation and advection, are included in Eq. 1. An analytical solution to the equation is possible under steady-state conditions if zero order

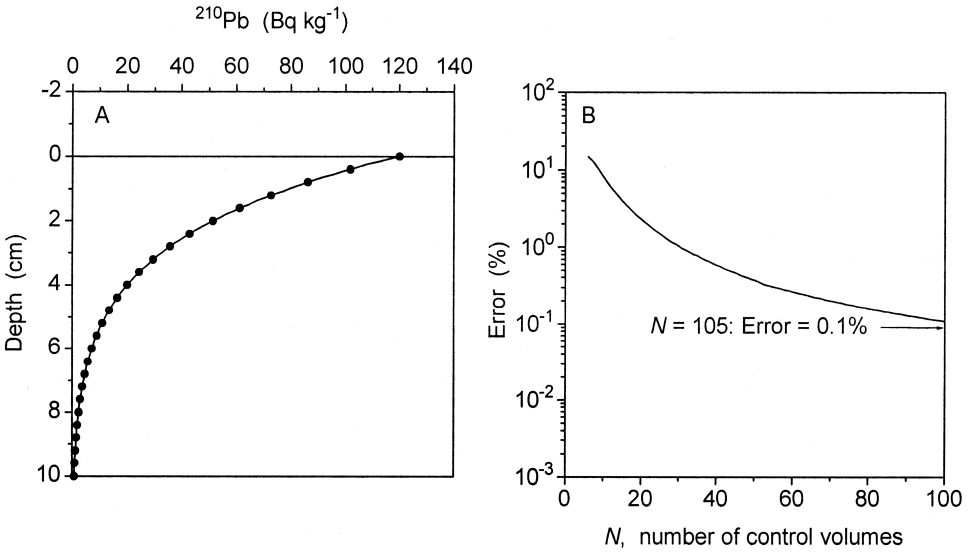

Figure 3. (A) Hypothetical steady state ^{210}Pb depth-profile defined analytically (dots) and simulated numerically by utilizing the algorithms CONSTANTS and CNEW (line). (B) The error of the numerical solution for different numbers of equally spaced control volumes separating the 0 to 10 cm depth interval.

production terms are neglected and if φ is assumed to be constant with depth. Under these conditions Eq. 1 simplifies to

$$\frac{d}{dx}\left(D_{Bs}\frac{dC}{dx}\right) - w\frac{dC}{dx} + \frac{R_2}{\rho_s(1-\varphi)}C = 0 \tag{20}$$

This equation describes for example a radioactive tracer, such as ^{210}Pb, that is supplied to a sediment surface at a constant rate, is transported to deeper sediment layers, and is disappearing through a first order decay. In this case the decay constant, λ, equals $-R_2/\rho_s(1-\varphi)$. Swaney (1999) showed that if D_{Bs} exhibits a parabolic decrease with depth as $D_{Bs} = D_{Bs0}(1 - x/L)^2$, the analytical solution to Eq. 20 in the 0 to L depth interval is

$$C = C_0\sqrt{\frac{L}{L-x}}\exp\left(\tfrac{1}{2}Pe\frac{x}{(L-x)}\right)\frac{K_\nu\left(\frac{1}{2}Pe\frac{L}{(L-x)}\right)}{K_\nu(\frac{1}{2}Pe)} \tag{21}$$

where C_0 is the concentration at the sediment surface, Pe is Peclet number equal to wL/D_{Bs0}, and K_ν is the modified Bessel function of the order ν and of the second kind where $\nu = \sqrt{\lambda L^2/D_{Bs0} + \frac{1}{4}}$. With values of L, D_{Bs0}, w, and λ of 10 cm, 0.05 cm^2 year^{-1}, 0.05 cm year^{-1}, and 0.0315 year^{-1}, a hypothetical ^{210}Pb profile was calculated from Eq. 21 (Fig. 3A). As in Example 1, the ^{210}Pb profile was simulated repeatedly for

increasing N and the error of the numerical solution was determined as the maximum deviation in the 0 to 10 cm depth interval from the analytical solution in percent of the sediment surface concentration (Fig. 3B). Also in this example each numerical solution was found in one "infinitely large" time step (1×10^{30} s). The error of the numerical solution decreases with increasing N (Fig. 3B), but not as pronounced as in Example 1. Errors of 1 and 0.1% were found for N equal to 31 and 105.

c. Example 3

As an example of nonsteady-state conditions, a conservative dissolved tracer that is supplied to a sediment from the overlying water is considered. An analytical solution to Eq. 1 is possible if irrigation is neglected and it is assumed that φ, D_s, and D_{Bw} are constant with depth. Under these conditions Eq. 1 simplifies to

$$\frac{\partial C}{\partial t} = (D_{Bw} + D_s)\frac{\partial^2 C}{dx^2} - u\frac{dC}{dx} \tag{22}$$

If the diffusive boundary layer is neglected and the tracer is absent in the sediment at time zero after which the tracer concentration is increased momentarily to a constant value at the sediment surface, the analytical solution to Eq. 22 is

$$C = \tfrac{1}{2} C_0 \left(\operatorname{erfc}\left(\frac{x - ut}{2\sqrt{(D_{Bw} + D_s)t}} \right) + \exp\left(\frac{xu}{(D_{Bw} + D_s)} \right) \operatorname{erfc}\left(\frac{x + ut}{2\sqrt{(D_{Bw} + D_s)t}} \right) \right) \tag{23}$$

where C_0 is the tracer concentration at the sediment surface (Bear and Verruijt, 1987). From Eq. 23 two hypothetical profiles were calculated, one where advection was neglected and one where advection was included with a downward directed velocity of 5 cm day^{-1} (Fig. 4A). Both profiles are valid for a time of 1 day after the water column concentration was increased and based on identical values of D_s and D_{Bw} of 5×10^{-6} cm^2 s^{-1}. Each of the profiles were simulated repeatedly over a range of N and time steps (Δt). The error of the numerical solution was determined as the maximum deviation in the 0 to 10 cm depth interval from the analytical solution is a percent of the concentration on the sediment surface (Figs. 4B and 4C). The error of the numerical solution decreases as expected with increasing N and Δt. As a result of numerical diffusion (i.e. Patankar, 1980) the error is approximately 10-fold larger for the profile influenced by advection. This example shows that transient simulations of advection-dominated systems demands relatively high numbers of control volumes to obtain an accurate numerical solution.

d. Example 4

As a more realistic example from a modeling point of view, the numerical solution was implemented in a simplified version of the dynamic diagenetic model put forward by Soetaert *et al*., (1996). The simplification consists of neglecting the nitrogen cycling. This leaves three reactions to be simulated (Table 2), oxic mineralization, anoxic mineralization, and oxidation of so-called reduced compounds, such as NH_4^+, Mn^{2+}, Fe^{2+}, and H_2S,

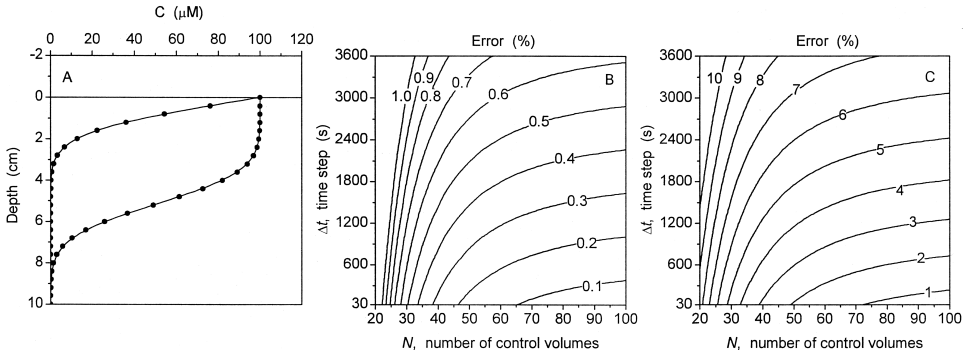

Figure 4. (A) Hypothetical transient depth-profiles after a one-day intrusion of a conservative dissolved tracer, defined analytically (dots) and simulated numerically by utilizing the algorithms CONSTANTS and CNEW (lines). The upper profile is influenced by diffusion only while the lower profile is the combined result of both diffusion and advection. (B) Iso-plot of errors for the numerically predicted, diffusion controlled, profile for different numbers of equally spaced control volumes separating the 0 to 10 cm depth interval and different time steps. (C) Iso-plot of errors for the numerically predicted, diffusion and advection controlled, profile for different numbers of equally spaced control volumes separating the 0 to 10 cm depth interval and different time steps. Note that errors are approximately 10 times larger for the profile under influence of both diffusion and advection.

which was modeled as one component and referred to as ODU (Oxygen Demanding Units). In addition to ODU, the model included O_2 plus a rapidly and a slowly decomposing pool of organic matter (OM). Furthermore, the active transport processes accounted for were molecular diffusion, bioturbation and burial as in the original model (Soetaert *et al.,* 1996). The regulation of all reactions was adopted from Berg *et al*., (2003) (Table 2). The model was applied to the Arctic sediment of one of the sites in Young Sound, Greenland, monitored intensively by Rysgaard and Berg (1996) and Rysgaard *et al*., (1998) through a full annual cycle. The site is located at 36 m depth, has a constant temperature year round, and a supply of OM that follows a dynamic pattern strongly affected by a short ice-free period in mid-summer.

As a realistic test example of the numerical solution, the model contains several rather challenging elements. For example, the reaction regulations are all clearly nonlinear and result in nonlinear production terms (Table 2). These production terms couple the mass conservation equations for the four simulated components, making all four equations nonlinear. In addition, both the depth and temporal scales of these components are markedly different. Specifically, O_2 penetrates only a few mm into the sediment and adjusts to dynamic changes on a time scale of 10 to 100 min, while decomposing OM reaches much larger sediment depths and adjusts to changes on a time scale of 10 to 100 years.

The numerical solution was implemented as follows. As an initial step, coefficients in the systems of equations, one system for each simulated component, were evaluated and the systems of equations were decomposed by the algorithm CONSTANTS, utilized only

Table 2. Simplified diagenetic reactions, their regulations, and the constituents included in Example 4. Simulated constituents are written in bold in the reactions. The symbols OM and ODU are used for organic matter and oxygen demanding units. A rapidly and a slowly decaying pool are utilized for OM.

Reaction 1

$$\mathbf{OM_f} + \mathbf{O_2} \xrightarrow{V_{1f}} CO_2 + \frac{1}{(C:N)} NH_4^+$$

$$\mathbf{OM_s} + \mathbf{O_2} \xrightarrow{V_{1s}} CO_2 + \frac{1}{(C:N)} NH_4^+$$

Reaction 2

$$\mathbf{OM_f} + \text{an oxidant} \xrightarrow{V_{2f}} CO_2 + \frac{1}{(C:N)} NH_4^+ + \mathbf{ODU}$$

$$\mathbf{OM_s} + \text{an oxidant} \xrightarrow{V_{2s}} CO_2 + \frac{1}{(C:N)} NH_4^+ + \mathbf{ODU}$$

Reaction 3

$$\mathbf{ODU} + \mathbf{O_2} \xrightarrow{V_3} \text{an oxidant}$$

Regulations

$$V_f = K_{\mathrm{OMf}}(1 - \varphi)\rho_s[\mathrm{OM_f}] \quad \text{and} \quad V_s = K_{\mathrm{OMs}}(1 - \varphi)\rho_s[\mathrm{OM_s}]$$

$$[O_2] \geq [O_{2\mathrm{lim}}]: \begin{cases} V_{1f} = V_f & \text{and} \quad V_{2f} = 0 \\ V_{1s} = V_s & \text{and} \quad V_{2s} = 0 \end{cases}$$

$$[O_2] < [O_{2\mathrm{lim}}]: \begin{cases} V_{1f} = V_f[O_2]/[O_{2\mathrm{lim}}] & \text{and} \quad V_{2f} = V_f - V_{1f} \\ V_{1s} = V_s[O_2]/[O_{2\mathrm{lim}}] & \text{and} \quad V_{2s} = V_s - V_{1s} \end{cases}$$

$$V_3 = K_3\varphi[\mathrm{ODU}][O_2]$$

Production terms

$$R_{\mathrm{OMf}} = -V_{1f} - V_{2f} \quad \text{and} \quad R_{\mathrm{OMs}} = -V_{1s} - V_{2s}$$

$$R_{O2} = -V_{1f} - V_{1s} - V_3$$

$$R_{\mathrm{ODU}} = V_{2f} + V_{2s} - V_3$$

once for each component. In each of the following time steps, first the reaction rates (V_{1f}, V_{1s}, V_{2f}, V_{2s}, V_3) and then the production terms (R_{OMf}, R_{OMs}, R_{O2}, R_{ODU}) were determined from known concentrations at time t (Table 2). Based on these production terms, new concentrations for time $t + \Delta t$ were determined by the algorithm CNEW, utilized once for each component in every time step.

This scheme relies on an explicit coupling between the mass balances through the production terms (R_{OMf}, R_{OMs}, R_{O2}, R_{ODU}). In order to avoid instabilities arising from this explicit coupling, especially in the initial phase of a simulation, none of the reaction rates were allowed to be negative. This was achieved by applying the intrinsic function MAX(a, b) which returns the maximum value of arguments a and b.

Site-specific quantities measured by Rysgaard and Berg (1996), Rysgaard *et al.* (1998)

Table 3. Input parameters in Example 4 and their origin.

	Parameter	Value	Source
1	Sedimentation rate	$w = 0.12$ cm year^{-1}	1, 2
2	Biodiffusivity for solutes	$x \leq 4$ cm: $D_{Bw} = 4.6 \times 10^{-6}$ cm^2 s^{-1} $x > 4$ cm: $D_{Bw} = 4.6 \times 10^{-6}\, e^{-0.35(x-4)}$ cm^2 s^{-1}	3, (2)
3	Biodiffusivity for solids	$D_{Bs} = D_{Bw}/12$	3, (2)
4	Molecular diffusivity at 0 °C	$D_{O2} = 11.7 \times 10^{-6}$ cm^2 s^{-1}	4
5	Molecular diffusivity at 0 °C	$D_{ODU} = 3.4 \times 10^{-6}$ cm^2 s^{-1}	5
6	Porosity	$\varphi = 0.631 + 0.207\, e^{-1.02x}$	6, (2)
7	Density of solid sediment	$\rho_s = 2.41$ g cm^{-3}	6
8	Diffusive boundary layer	$\delta_D = 0.03$ cm	6, (2)
9	Boundary condition	$F_{OM} = 2300$ mmol m^{-2} year^{-1}	6
10	Boundary condition	$[O_2]_{x=-0.03} = 389$ μM	6
11	Boundary condition	$[ODU]_{x=-0.03} = 0$ μM	2
12	Limiting concentration.	$[O_2]_{lim} = 20$ μM	7, (2)
13	Rate constant	$K_{OMf} = 2.0 \times 10^{-6}$ s^{-1}	*
14	Rate constant	$K_{OMs} = 3.0 \times 10^{-9}$ s^{-1}	*
15	Rate constant	$K_3 = 1.1 \times 10^{-6}$ μM^{-1} s^{-1}	7, (2)
16	Ratio	$F_{OMf}/F_{OMs} = 0.5$	8
17	Ratio	$F_{OM\ peak}/F_{OM\ base} = 6$	*

1) Rysgaard *et al.* (1996); 2) Berg *et al.* (2003); 3) Berg *et al.* (2001); 4) Broecker and Peng (1974); 5) Li and Gregory (1974); 6) Rysgaard *et al.* (1998); 7) Van Cappellen and Wang (1996); 8) Soetaert *et al.* (1996); *This study.

and Berg *et al*. (2001) were used for many input parameters to the model (1, 2, 3, 6, 7, 8, 9, 10, 11, Table 3). The limiting O_2 concentration (12, Table 3) used in the regulation of the reactions was taken from Van Cappellen and Wang (1996) and Berg *et al*., (2003) as was the rate constant for Reaction 3 (15, Table 3). This rate constant was used in these studies for the reaction of Fe^{2+} with O_2 and by adopting this constant here, it was implicitly assumed that the ODU pool consists mostly of Fe^{2+} in accordance with the findings of Berg *et al*. (2003) at this site. The distribution of the OM supply between the rapidly and the slowly decomposing OM pools (16, Table 3) was taken from Soetaert *et al*. (1996). All these parameters were kept constant in all simulations.

The last three input parameters to be assigned, the rate constants for the two OM pools and the time dependant OM flux supplied to the sediment, were given values by comparing simulated and measured results repetitively and adjusting the three input parameters. Based on the measured pattern of O_2 fluxes (Fig. 5B) and also two OM sedimentation rates (Fig. 5A) reported by Rysgaard *et al*. (1998), it was assumed that the variation of the OM flux over the year consists of a base contribution plus a short peak summer contribution with a duration of 1 month (Fig. 5A). With a known annual supply of OM to the sediment (9, Table 3) also reported by Rysgaard *et al.* (1998), the dynamic OM flux was uniquely defined by the ratio between the peak summer contribution and the base contribution (17, Table 3).

Despite the simplicity of the model, a good agreement was achieved for the O_2 uptake

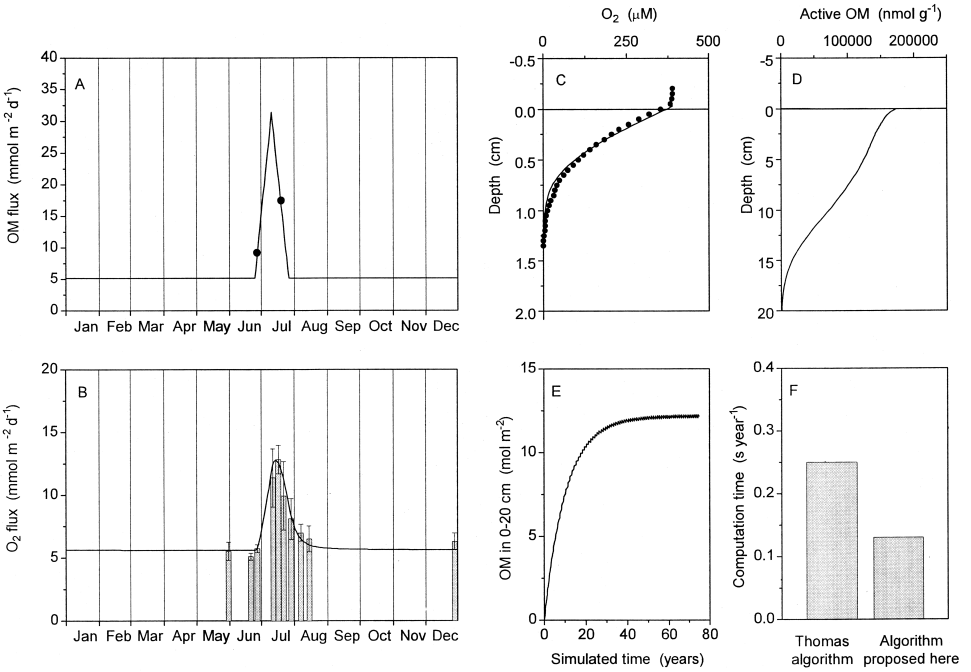

Figure 5. Application of a dynamic, multi-component, and nonlinear model of organic matter and nutrient diagenesis to an Arctic sediment (Table 2 and 3) by utilizing the algorithms CONSTANTS and CNEW. (A) Supply of organic matter to the sediment over the year found in the model parameterization (line) and two measured organic matter fluxes (dots). (B) Simulated (line) and measured (bars, errors represent ± 1 SE, $n = 6$) O_2 uptake over the year. (C) Simulated (line) and measured (dots) O_2 depth-profile in mid August. (D) Simulated depth-profile of decomposing organic matter. (E) Simulated depth-integrated organic matter content through 75 years of simulated time. Initial condition in the simulation was a sediment absent of organic matter. (F) Computation time required per simulated year using the standard Thomas algorithm as equation solver and the algorithm presented in this study. The results were produced on a 2.0 GHz Pentium M PC.

throughout the year (Fig. 5B). A similarly good agreement was obtained with the measured O_2 concentration profile determined by Rysgaard *et al*., (1998) in mid August (Fig. 5C).

All simulations were based on a time step of 1 hour and a separation of the diffusive boundary layer and the upper 20 cm of the sediment into 100 control volumes. This depth was required to diminish the slow pool of OM to close to zero concentrations (Fig. 5D). The upper 1 cm of the sediment was separated into equally sized control volumes of 0.03 cm after which the control volume size was gradually increased with depth. This discretization in time and space was found to be adequate to obtain precise numerical solutions in an additional simulation performed with a time step of 15 min and 200 control volumes which gave the same annual O_2 uptake within 0.04%.

From initial conditions of zero OM, O_2, and ODU in the sediment, 75 years of simulated

time were required to build up the OM pools to quasi-stationary conditions on a year to year basis (Fig. 5E). Even though some 50 simulations were performed in this model parameterization, the 75 years of simulated time did not lead to prohibitive computation times as the model was running at the speed of 0.13 s per simulated year on a 2.0 GHz Pentium M PC (Fig. 5F). This good performance was the combined result of three factors. Firstly, the implicit formulation in the numerical solution allowed a relatively large time step to be used. Specifically, the time step was 100 times larger than the maximum allowed critical time step of explicit formulations (see above). Secondly, the separation of the forward and the back substitution in the numerical solution allowed the system of 100 equations per simulated component to be decomposed only once, after which new concentrations were found with little computational effort in every time step. Thirdly, the novel implementation of boundary conditions allowed the values of boundary conditions to vary as simulations progressed without requiring new decompositions of the systems of equations. This characteristic was clearly taken advantage of here with respect to the imposed OM flux (Fig. 5A). An additional simulation, performed with the standard Thomas algorithm as equation solver (Eqs. 12 and 13) instead of our algorithms (Eqs. 14 and 15), required the double amount of computation time (Fig. 5F). It should be emphasized that this simulation with the standard Thomas algorithm also was optimized with respect to computation time by only calculating the constants AA_j, BB_j and CC_j (Eq. 9) once. Because the number of numeric operations in multi-component diagenetic models typically varies linearly with the number of species accounted for, this factor of two conservatively represents the computational efficiency to be gained over the Thomas algorithm by using the algorithms proposed in this study.

The explicit coupling used between the mass balances for each component represents the simplest possible way to overcome the inherent nonlinearities in multi-component diagenetic models. A more advanced implicit coupling that would allow markedly larger time steps than used here is also possible. Although this would require iterations to be performed in every time step to overcome these nonlinearities, it would lead to even faster overall computation times. In such formulations, the algorithms CONSTANTS and CNEW can also be used equally as effectively. Details on how to formulate such iterative schemes most effectively are for example given by Patankar (1980) and Berg (1999).

4. Summary and conclusion

Many researchers modeling species transformations in aquatic sediments have found that computation times of numerical solutions can become prohibitively long. In many cases, this is either due to inefficient algorithms or to algorithms being misapplied to problems inappropriate to them. The numerical solution presented here is suited to both single and multi-component models, and aims to minimize this problem, taking advantage of three factors:

1. The numerical solution is based on an implicit formulation of the discretization equation which provides a versatile approach for solving transient problems using

relatively large time steps, and at the same time, allowing steady-state solutions to linear problems to be produced in one single "infinitely large" time step.

2. Care has been taken to re-calculate model variables only when necessary, i.e., as a simulation progresses when or if they change. For example, in transient solutions all non-essential numerical operations are eliminated from the repetitive time loop. Consequently, the numerical solution consists of two algorithms, CONSTANTS and CNEW, one that decomposes the discretization matrix once and one that subsequently can be utilized numerous times with minimal computational effort. In transient solutions, this will be in every time step.

3. The algorithms are uniquely formulated to allow the values of boundary conditions to vary as a simulation progresses without requiring new decompositions of the discretization matrix.

The combined effect of these features can reduce computation times significantly relative to procedures commonly used for modeling species transformations in aquatic sediments. Although the last example presented above focuses on a relatively simple diagenetic model, it illustrates clearly the potential benefits in terms of computation times that can be achieved with this numerical solution.

Available Software

Copies of the algorithms CONSTANTS and CNEW, coded in FORTRAN 90, can be obtained free of charge from the corresponding author. For optimal performance, the algorithms should be applied in double precision.

Acknowledgments. We thank D. Burdige and one anonymous reviewer for their constructive reviews of this paper. This study was supported by grants from the University of Virginia and the Danish National Science Research Councils (contract nos. 9501025 and 9700224).

APPENDIX A

Approximation of fluxes

As illustrated by Patankar (1980) a first evaluation of flux-approximating schemes can be achieved by comparison with the analytical solution of the one-dimensional steady state mass-conservation equation that accounts for diffusion and advection. This approach is adapted here, and complemented with computation times for evaluation of the schemes on modern computer processors. The one-dimensional steady state mass-conservation equation including diffusive and advective transport contributions can be written in the form

$$\frac{dJ}{dx} = 0$$
$$J = -H_2 \frac{dC}{dx} + H_3 C \tag{A1}$$

If H_2 and H_3 are constant with depth, Eq. A1 have the analytical solution (i.e. Patankar, 1980 or Boudreau, 1997)

$$\left.\begin{array}{ll} x = 0: & C = C_0 \\ x = L: & C = C_L \end{array}\right\} \Rightarrow J = H_3\left(C_0 + \frac{C_0 - C_L}{\exp\left(\frac{H_3}{H_2} L\right) - 1} \right) \tag{A2}$$

Assuming for now that Δx_j is constant with depth and referred to as Δx, and using this solution to express the intermediate combined diffusive-advective flux, $J_{j-1/2}$, at the boundary between control volume j-1 and j, gives

$$J_{j-1/2} = H_3\left(C_{j-1} + F(P)\, \frac{C_{j-1} - C_j}{P} \right) \tag{A3}$$

where the function $F(P)$ is given by

$$F(P) = \frac{P}{\exp(P) - 1} \tag{A4}$$

and where P is the Peclet number defined as

$$P = \frac{H_3}{H_2}\, \Delta x \tag{A5}$$

Numerical solutions of Eq. 1 can be produced by expressing the fluxes between control volumes according to Eq. A3. The expression of $J_{j-1/2}$ in combination with Eq. A4 is often referred to as the exponential scheme based on the expression for $F(P)$ and was first put forward by Spalding (1972) and later by Fiadeiro and Veronis (1977). At the time when the exponential scheme was defined, the exponential function was time consuming to evaluate on computers of the day. In addition, $F(P)$ needs special attention in its evaluation as it contains a singularity for $P = 0$. For those reasons, researchers derived new schemes relying on approximations of $F(P)$ that were markedly faster to evaluate (i.e. Spalding, 1972; Patankar, 1981; Berg, 1985). The most popular schemes, including the classic central difference and upwind schemes (Courant *et al*., 1952), are shown in Table A1 along with the normalized computation time for their evaluation on a 2.0 GHz Pentium M PC. As an example of derivation, the central difference approximation of $F(P)$ can be derived by approximating the intermediate flux as $J_{j-1/2} = -H_2(C_j - C_{j-1})/\Delta x + H_3(C_j + C_{j-1})/2$ which is equivalent to Eq. A3 if $F(P) = 1 - 0.5P$ (Table A1). The exact function $F(P)$ and its approximations are illustrated in Figure A1.

The central difference scheme provides a good approximation of $F(P)$ only for small values of P, and is the only scheme in which the divergence from $F(P) \rightarrow \infty$ as $P \rightarrow \pm\infty$ (Fig. 1A). This characteristic explains why instabilities occur when using central difference approximation for advection-dominated systems ($|P| \gg 0$). The normalized computation times (Table A1) show that the power law scheme which was used extensively in the 1980s and 1990s, is outdated today as its evaluation is more time consuming

Table A1. Formulations of the function $F(P)$ in different schemes. The formulations are given on a form that ensures minimal use of computation time in their evaluations. The normalized evaluation times are valid for a 2.0 GHz Pentium M PC. The two intrinsic functions, SIGN and MAX, each have two arguments, and are standard functions in FORTRAN. Function SIGN performs a sign transfer by returning the absolute value of the first argument multiplied by the sign of the second argument. Function MAX returns the maximum value of the arguments.

Scheme	Approximations of $F(P) = P/(\exp(P) - 1)$	Normalized time for one evaluation	Reference
Exact	$P_{help} = \text{SIGN}(\text{MAX}(10^{-5}, \lvert P\rvert), P)$ $F(P) = P_{help}/(\exp(P_{help}) - 1)$	1.0	1), 2)
Power law	$F(P) = \text{MAX}(0, (1 - 0.1\lvert P\rvert)^5) + \text{MAX}(0, -P)$	1.2	3)
Hyperbolic	$F(P) = \text{MAX}(0, 8/(4 + \lvert P\rvert) - 1) + \text{MAX}(0, -P)$	0.093	4)
Hybrid	$F(P) = \text{MAX}(0, -P, 1 - 0.5P)$	0.062	1)
Upwind	$F(P) = \text{MAX}(1, 1 - P)$	0.047	5)
Central	$F(P) = 1 - 0.5P$	0.037	

1) Spalding, 1972, 2) Fiadeiro and Veronis, 1977, 3) Patankar, 1981, 4) Berg, 1985, 5) Courant *et al.,* 1952

than the exact scheme. Both the hyperbolic and the hybrid scheme appear to be good choices based on their good approximation of $F(P)$ (Fig. A1) in combination with their relatively short evaluation times. However, it should be noted that the evaluation time

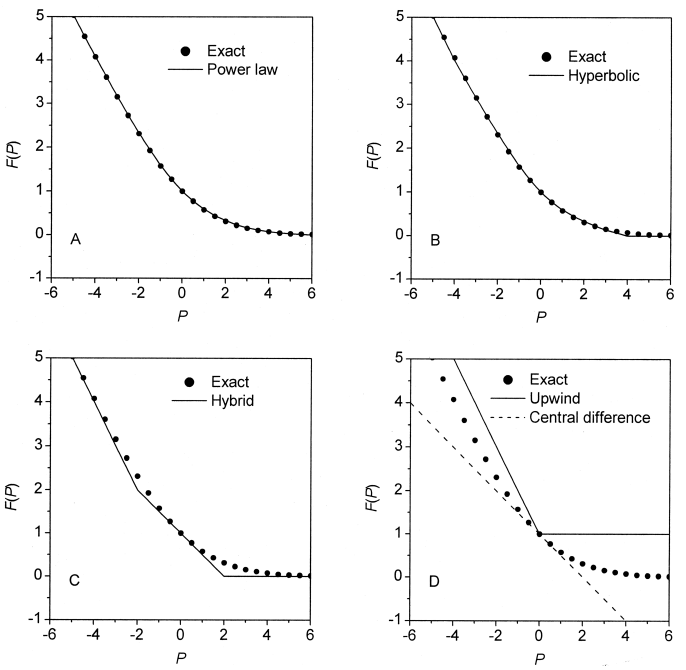

Figure A1. The exact function $F(P)$ and its approximation in alternate schemes.

should affect the choice of scheme only in model formulations where numerous evaluations of $F(P)$ are expected.

In this brief comparison it was assumed that Δx, H_2, and H_3 are constant with depth. This is only true for H_3 in Eq. 3, and an expression similar to Eq. A3 where variations in Δx and H_2 are accounted for is derived from Eq. A2 as follows. Assuming that the grid point values of H_2 prevail throughout control volumes as representative mean values, the flux $J_{j-1/2}$ can be expressed for control volume j-1 by the variables C_{j-1}, $C_{j-1/2}$, Δx_{j-1}, $H_{2\,j-1}$, and H_3 as

$$J_{j-1/2} = H_3\left(C_{j-1} + \frac{C_{j-1} - C_{j-1/2}}{\exp\left(\frac{H_3}{H_{2\,j-1}}\frac{1}{2}\Delta x_{j-1}\right) - 1}\right) \tag{A6}$$

The same flux can similarly be expressed for control volume j by the variables $C_{j-1/2}$, C_j, Δx_j, $H_{2\,j}$, and H_3 as

$$J_{j-1/2} = H_3\left(C_{j-1/2} + \frac{C_{j-1/2} - C_j}{\exp\left(\frac{H_3}{H_{2\,j}}\frac{1}{2}\Delta x_j\right) - 1}\right) \tag{A7}$$

Eliminating $C_{j-1/2}$ by combining these two expressions leads to (equivalent to Eq. A3)

$$J_{j-1/2} = H_3\left(C_{j-1} + F(P_{j-1/2})\,\frac{C_{j-1} - C_j}{P_{j-1/2}}\right) \tag{A8}$$

where the function $F(P_{j-1/2})$ is given by (equivalent to Eq. A4)

$$F(P_{j-1/2}) = \frac{P_{j-1/2}}{\exp(P_{j-1/2}) - 1} \tag{A9}$$

and the Peclet number $P_{j-1/2}$ is defined as the simple average of P_{j-1} and P_j (equivalent to Eq. A5)

$$P_{j-1/2} = \frac{1}{2}\left(\frac{H_3\Delta x_{j-1}}{H_{2\,j-1}} + \frac{H_3\Delta x_j}{H_{2\,j}}\right) \tag{A10}$$

or alternatively as

$$P_{j-1/2} = \frac{H_3}{H_{2\,j-1/2}}\,\frac{1}{2}\,(\Delta x_{j-1} + \Delta x_j) \tag{A11}$$

where $H_{2\,j-1/2}$ is given by the weighted harmonic mean of $H_{2\,j-1}$ and $H_{2\,j}$ as

$$H_{2\,j-1/2} = \frac{H_{2\,j-1}H_{2\,j}(\Delta x_{j-1} + \Delta x_j)}{\Delta x_{j-1}H_{2\,j} + \Delta x_j H_{2\,j-1}} \tag{A12}$$

The general expression of the flux $J_{j-1/2}$ over the boundary between control volume j-1 and j is defined by the two variables, $F_{1\,j}$ and $F_{2\,j}$, (Eq. 5). These variables can now be derived from Eq. A8 as

$$F_{1\,j} = -F(P_{j-1/2})\,\frac{H_{2\,j-1/2}}{\frac{1}{2}(\Delta x_{j-1} + \Delta x_j)}$$
$$F_{2\,j} = -F_{1\,j} + H_3 \tag{A13}$$

where the function $F(P_{j-1/2})$ is taken from Table A1.

APPENDIX B

The algorithm "CONSTANTS"

Below is listed the input to and the output from the algorithm CONSTANTS, followed by a summary of the algorithm. Units of input and output variables are included as an example. Other units can be used as long as they are mutually consistent.

Input:

L	[-]	Number of first control volume (=1 or M, see Fig. 1)
M	[-]	Number of control volume at the sediment surface (see Fig. 1)
N	[-]	Number of last control volume (see Fig. 1)
Δt	[s]	Time step
Δx_j	[cm]	Size of control volumes
φ_j	[-]	Porosity
D	[cm^2 s^{-1}]	Diffusivity in water
$D_{Bw\,j}$	[cm^2 s^{-1}]	Biodiffusivity for solutes
$D_{Bs\,j}$	[cm^2 s^{-1}]	Biodiffusivity for solids
ρ_s	[g cm^{-3}]	Density of sediment
α_j	[s^{-1}]	Irrigation coefficient
$R_{2\,j}$	[s^{-1}]	Production rates
$(\varphi u)_x$	[m s^{-1}]	Porosity times porewater velocity (constant with depth)
$((1-\varphi)w)_x$	[m s^{-1}]	One minus porosity times burial velocity (constant with depth)
ξ	[-]	Equal to 1 for solutes and equal to 0 for solids
κ	[cm^3 g^{-1}]	Coefficient (=0, 1 or K' where K' is the adsorption constant)
FL_0	[-]	Flag for choosing the expression for D_s (=1, 2, 3, 4 or 5)
FL_1	[-]	Flag for choosing the upper boundary condition (=1, 2, or 3)
FL_2	[-]	Flag for choosing the lower boundary condition (=1, 2, or 3)

Output:

AA_j	[cm s^{-1}]	Input to CNEW
EE_j	[cm s^{-1}]	Input to CNEW
FF_j	[cm s^{-1}]	Input to CNEW
NN_j	[s cm^{-1}]	Input to CNEW
PP_j	[-]	Input to CNEW
$F_{1\,j}$	[cm s^{-1}]	Constants for calculation of flux (Eq. 5)
$F_{2\,j}$	[cm s^{-1}]	Constants for calculation of flux (Eq. 5)

Calculation of D_{sj} depending of the flag FL_0:

$$\left.\begin{aligned}
&FL_0 = 1: \quad D_{sj} = \varphi_j D \\
&FL_0 = 2: \quad D_{sj} = \varphi_j^2 D \\
&FL_0 = 3: \quad D_{sj} = \frac{D}{1 + 2(1 - \varphi_j)} \\
&FL_0 = 4: \quad D_{sj} = \frac{D}{1 + 3(1 - \varphi_j)} \\
&FL_0 = 5: \quad D_{sj} = \frac{D}{1 - \ln(\varphi_j^2)}
\end{aligned}\right\} \quad (j = L \rightarrow N) \tag{B1}$$

Calculation of H_{1j}, H_{2j}, H_3, and H_{4j}:

$$\left.\begin{aligned}
H_3 &= \xi(\varphi u)_x + \rho_s((1 - \varphi)w)_x \kappa \\
H_{1j} &= \xi\varphi_j + \rho_s(1 - \varphi_j)\kappa \\
H_{2j} &= \xi\varphi_j(D_{Bwj} + D_{sj}) + \rho_s(1 - \varphi_j)D_{Bsj}\kappa \\
H_{4j} &= \xi\varphi_j\alpha_j
\end{aligned}\right\} \quad (j = L \rightarrow N) \tag{B2}$$

Calculation of F_{1j} and F_{2j}. Note that special precautions are taken to avoid division by zero. The function MAX(a, b) is a standard function in FORTRAN and returns the maximum value in the argument list. The number 10^{-36} is close to the smallest value that can be represented in single precision in FORTRAN.

$$\left.\begin{aligned}
H_{2j-1/2} &= \frac{H_{2j-1}H_{2j}(\Delta x_{j-1} + \Delta x_j)}{\mathrm{MAX}(10^{-36}, \Delta x_{j-1}H_{2j} + \Delta x_j H_{2j-1})} \\
P_{j-1/2} &= \frac{H_3}{\mathrm{MAX}(10^{-36}, H_{2j-1/2})}\frac{1}{2}(\Delta x_{j-1} + \Delta x_j) \\
F(P_{j-1/2}) &= \mathrm{MAX}(0, 8/(4 + |P_{j-1/2}|) - 1) + \mathrm{MAX}(0, -P_{j-1/2}) \\
F_{1j} &= -F(P_{j-1/2})\frac{H_{2j-1/2}}{\frac{1}{2}(\Delta x_{j-1} + \Delta x_j)} \\
F_{2j} &= -F_{1j} + H_3
\end{aligned}\right\} \quad (j = L + 1 \rightarrow N) \tag{B3}$$

Calculation of the coefficients AA_j, BB_j and CC_j in the tri-diagonal system of equations:

$$\left.\begin{aligned}
AA_j &= F_{2j} \\
BB_j &= F_{1j} - F_{2j+1} - H_{4j}\Delta x_j + R_{2j}\Delta x_j - H_{1j}\frac{\Delta x_j}{\Delta t} \\
CC_j &= -F_{1j+1}
\end{aligned}\right\} \quad (j = L + 1 \rightarrow N - 1) \tag{B4}$$

Calculation of the coefficients BB_L and CC_L for the upper boundary condition. The type of boundary condition is specified by the flag FL_1:

$$\begin{aligned} FL_1 = 1: &\quad BB_L = 1; \quad CC_L = 0 \\ FL_1 = 2: &\quad BB_L = F_{2\,L+1}; \quad CC_L = F_{1\,L+1} \\ FL_1 = 3: &\quad BB_L = -\frac{2}{\Delta x_{L+1}}; \quad CC_L = -BB_L \end{aligned} \tag{B5}$$

Calculation of the coefficients AA_N and BB_N for the lower boundary condition. The type of boundary condition is specified by the flag FL_2:

$$\begin{aligned} FL_2 = 1: &\quad AA_N = 0; \quad BB_N = 1 \\ FL_2 = 2: &\quad AA_N = F_{2\,N}; \quad BB_N = F_{1\,N} \\ FL_2 = 3: &\quad AA_N = -\frac{2}{\Delta x_{N-1}}; \quad BB_N = -AA_N \end{aligned} \tag{B6}$$

Calculation of the coefficients NN_j and PP_j in the forward substitution:

$$\begin{aligned} NN_L &= \frac{1}{BB_L}; \quad PP_L = -CC_L NN_L \\ NN_j &= \frac{1}{BB_j + AA_j PP_{j-1}} \\ PP_j &= -CC_j NN_j \end{aligned} \Bigg\} \quad (j = L+1 \rightarrow N-1) \tag{B7}$$

$$NN_N = \frac{1}{BB_N + AA_N PP_{N-1}}$$

Calculation of the coefficients EE_j and FF_j used to calculate the right hand side in the tri-diagonal system of equations:

$$\begin{aligned} EE_j &= H_{1\,j}\frac{\Delta x_j}{\Delta t} \\ FF_j &= H_{4j}\Delta x_j \end{aligned} \Bigg\} \quad (j = L+1 \rightarrow N-1) \tag{B8}$$

APPENDIX C

The algorithm "CNEW"

Below is listed the input to and the output from the algorithm CNEW, followed by a summary of the algorithm. Units of input and output variables are included as an example. Other units can be used as long as they are mutually consistent.

Input:

L	[-]	Number of first control volume (=1 or M, see Fig. 1)
N	[-]	Number of last control volume (see Fig. 1)
Δx_j	[cm]	Size of control volumes
AA_j	[cm s^{-1}]	Input from CONSTANTS
EE_j	[cm s^{-1}]	Input from CONSTANTS
FF_j	[cm s^{-1}]	Input from CONSTANTS

Input (continued):

NN_j	[s cm^{-1}]	Input from CONSTANTS
PP_j	[-]	Input from CONSTANTS
C_0	[nmol cm^{-3}]	Known water column concentration
C_j^n	Solute: [nmol cm^{-3}] Solid: [nmol g^{-1}]	Known concentrations at the old time level
$R_{1\,j}$	[nmol cm^{-3} s^{-1}]	Production rates
BC_L	$FL_1 = 1$: [nmol cm^{-3}] or [nmol g^{-1}] $FL_1 = 2$: [nmol cm^{-2} s^{-1}] $FL_1 = 3$: [nmol cm^{-4}] or [nmol g^{-1} cm^{-1}]	Known boundary condition at top
BC_N	$FL_2 = 1$: [nmol cm^{-3}] or [nmol g^{-1}] $FL_2 = 2$: [nmol cm^{-2} s^{-1}] $FL_2 = 3$: [nmol cm^{-4}] or [nmol g^{-1} cm^{-1}]	Known boundary condition at bottom

Output:

C_j^{n+1}	Solute: [nmol cm^{-3}] Solid: [nmol g^{-1}]	New concentrations at the new time level

Calculation of the coefficients QQ_j:

$$\begin{aligned} QQ_L &= BC_L NN_L \\ QQ_j &= (-EE_j C_j^n - FF_j C_0 - R_{1\,j}\Delta x_j - AA_j QQ_{j-1})NN_j \quad (j = L+1 \rightarrow N-1) \end{aligned} \tag{C1}$$

Calculation of the new concentrations C_j^{n+1}:

$$\begin{aligned} C_N^{n+1} &= (BC_N - AA_N QQ_{N-1})NN_N \\ C_j^{n+1} &= PP_j C_{j+1}^{n+1} + QQ_j \quad (j = N-1 \rightarrow L) \end{aligned} \tag{C2}$$

REFERENCES

Bear, J. and A. Verruijt. 1987. Modeling Groundwater Flow and Pollution. Theory and applications of Transport in Porous Media. Kluwer Academic Publisher Group, 414 pp.

Berg, P. 1985. Discretization of the general transport equation presented in cylindrical coordinates, *in* Proceedings of the first Danish-Polish workshop on modeling heat flow and fluid flow problems, M. Dytczak and P. N. Hansen, eds., Thermal Insulation Laboratory, Technical University of Denmark, 95–105.

—— 1999. Long-term simulation of water movement in soils using mass-conserving procedures. Adv. Water Resources, *22*, 419–430.

Berg, P., N. Risgaard-Petersen and S. Rysgaard. 1998. Interpretation of measured concentration profiles in sediment pore water. Limnol. Oceanogr., *43,* 1500–1510.

Berg, P., S. Rysgaard, P. Funch and M. K. Sejr. 2001. Effects of bioturbation on solutes and solids in marine sediments. Aq. Micro. Ecol., *26*, 81–94.

Berg, P., S. Rysgaard and B. Thamdrup. 2003. Dynamic modeling of early diagenesis and nutrient cycling. A case study in an Arctic marine sediment. Amer. J. Sci., *303*, 905–955.

Berner, R. A. 1980. Early Diagenesis. A Theoretical approach, Princeton University Press, 241 pp.

Boudreau, B. P. 1996. A method-of-lines code for carbon and nutrient diagenesis in aquatic sediments. Comp.Geosci., *22*, 479–496.

—— 1997. Diagenetic Models and Their Implementation. Springer-Verlag, 414 pp.

Broecker, W. S. and T.-H. Peng. 1974. Gas exchange rates between air and sea. Tellus, *26*, 21– 35.

Courant, R., E. Isaacson and M. Rees. 1952. On the solution of non-linear hyperbolic differential equations by finite differences. Comm. Pure Appl. Math., *5*, 243–255.

Dhakar, S. P. and D. J. Burdige. 1996. A coupled, non-linear, steady state model for early diagenetic processes in pelagic sediments. Amer. J. Sci., *296*, 296–330.

Fiadeiro. M. E. and G. Veronis. 1977. On weighted-mean schemes for finite-difference approximation to the advection-diffusion equation. Tellus, 29, 512–522.

Huyakorn, P. S. and C. F. Pinder. 1983. Computational Methods of Subsurface Flow. Princeton University Press, 473 pp.

Iversen, N. and B. B. Jørgensen. 1993. Measurements of the diffusion coefficients in marine sediments: influence of porosity. Geochim., Cosmochim. Acta, *57*, 571–578.

Li, Y.-H. and S. Gregory. 1974. Diffusion of ions in sea water and deep-sea sediments. Geochim., Cosmochim. Acta, *38*, 703–714.

Luff, R., K. Wallmann, S. Grandel and M. Schlüter. 2000. Numerical modeling of benthic processes in the deep Arabian Sea. Deep-Sea Res. II, *47*, 3039–3072.

Meysman, F. J. R., J. J. Middelburg, P. M. J. Herman and C. H. R. Heip. 2003. Reactive transport in surface sediments. II. Media: an object-oriented problem-solving environment for early diagenesis. Comp.Geosci., *29*, 301–318.

Meile, C., C. M. Koretsky and P. Van Cappellen. 2001. Quantifying bioirrigation in aquatic sediments: An inverse modeling approach. Limnol. Oceanogr., *46*, 164–177.

Mulsow, S., B. P. Boudreau and J. N. Smith. 1998. Bioturbation and porosity gradients. Limnol. Oceanogr., *43*, 1–9.

Patankar, S. V. 1980. Numerical Heat Transfer and Fluid Flow. McGraw Hill, 197 pp.

—— 1981. Calculation procedure for two-dimensional elliptic situations. Num Heat Transfer, *4*, 409–425.

Rysgaard, S. and P. Berg. 1996, Mineralization in a northeastern Greenland sediment: mathematical modelling, measured sediment pore water profiles and actual activities. Aq. Micro. Ecol., *11*, 297–305.

Rysgaard, S., B. Thamdrup, N. Risgaard-Petersen, H. Fossing, P. Berg, P. B. Christensen and T. Dalsgaard. 1998. Seasonal carbon and nitrogen mineralization in a high-Arctic coastal marine sediment, Young Sound, Northeast Greenland. Mar. Ecol. Prog. Ser., *175*, 261–276.

Soetaert, K., P. M. J. Herman and J. J. Middelburg. 1996, A model of early diagenetic processes from the shelf to abyssal depths. Geochim., Cosmochim. Acta, *60*, 1019–1040.

Spalding, D. B. 1972. A novel finite-difference formulation for differential expression involving both first and second derivatives. Inter. J. Num. Methods, England, *4*, 551–559.

Swaney, D. P. 1999. Analytical solution of Boudreau's equation for a tracer subject to food-feedback bioturbation. Limnol. Oceanogr., *44*, 697–698.

Ullman, W. J. and R. C. Aller. 1982. Diffusion coefficients in nearshore marine sediments. Limnol. Oceanogr., *27*, 552–556.

Van Cappellen, P. and Y. Wang. 1996. Cycling of iron and manganese in surface sediments: A general theory for the coupled transport and reaction of carbon, oxygen, nitrogen, sulfur, iron, and manganese. Amer. J. Sci., *296*, 197–243.

Received: *12 December, 2006*; revised: *27 February, 2007*.